catalysts

MDPI

Article

Propane Dehydrogenation on Co-N-C/SiO_2 Catalyst: The Role of Single-Atom Active Sites

Aleksey N. Chernov, Vladimir I. Sobolev, Evgeny Yu. Gerasimov and Konstantin Yu. Koltunov *

Boreskov Institute of Catalysis, Russian Academy of Sciences, Pr. Akademika Lavrentieva, 5, 630090 Novosibirsk, Russia

* Correspondence: koltunov@catalysis.ru; Tel.: +7-383-3269465

Abstract: Recently, significant attention has been drawn to carbon materials containing cobalt coordinated to nitrogen, as the promising inexpensive catalysts of a wide range of applications. Given that non-oxidative propane dehydrogenation to propylene (PDH) is also becoming increasingly important, we present the results on PDH over Co-N-C/SiO_2 composites. The latter were prepared by pyrolysis of silicone gel enriched with Co(II) salt and triethanolamine. According to XRD, HRTEM and XPS characterizations, the resulting materials consist of metallic cobalt nanoparticles of about 5 to 10 nm size and subnano-sized cobalt species (cobalt single atom sites coordinated to nitrogen/carbon), which are uniformly distributed in mesoporous silica of high specific surface area (up to 500 $m^2\ g^{-1}$). The composites demonstrated significant catalytic activity in PDH, which was examined under typical reaction conditions (600 °C, 1 atm) using a fixed bed flow reactor. The subnano-sized Co centers proved to be the real active catalytic sites responsible for the target reaction, while carbon deposition induced by Co nanoparticles provided the catalyst deactivation. It is shown that the catalyst can be reactivated by the treatment with oxygen, which, in addition, notably increases selectivity to propylene (up to 98%) and enhances the catalyst stability in the next operation cycle. This remarkable change in catalytic behavior is shown to be due to the dramatic structural modification of the catalyst upon high-temperature oxidation.

Keywords: propylene; propane dehydrogenation; cobalt–nitrogen–carbon catalyst; mechanistic aspects

Citation: Chernov, A.N.; Sobolev, V.I.; Gerasimov, E.Y.; Koltunov, K.Y. Propane Dehydrogenation on Co-N-C/SiO_2 Catalyst: The Role of Single-Atom Active Sites. *Catalysts* **2022**, *12*, 1262. https://doi.org/10.3390/catal12101262

Academic Editors: Maria Jaworska and Piotr Lodowski

Received: 15 September 2022
Accepted: 13 October 2022
Published: 17 October 2022

1. Introduction

Propylene is an important basic chemical in the petrochemical industry, which is produced largely by the oil-cracking approach along with other olefins [1]. Besides, a more atomic efficient technique, such as non-oxidative propane dehydrogenation to propylene (PDH), becomes of growing significance [1–10]. Currently, commercial PDH processes are based on the use of Pt/Al_2O_3 or CrO_x/Al_2O_3 catalysts, which, however, have a number of drawbacks related to the high cost and difficult reactivation of the platinum catalyst and unacceptable environmental impact of the chromium catalyst. It is therefore not surprising that significant efforts have been made to develop alternative PDH catalysts, represented mainly by supported transition metal oxides [2–10]. Carbon-based materials are also of particular interest in this regard, especially those enriched with heteroelements (N, P, B) or comprising transition metal complexes with heteroatoms [11–19]. These include, inter alia, Co-N-C-based materials, which demonstrated significant catalytic activity and selectivity to propylene in the PDH reaction [20–25].

Notably, the Co@NC composites themselves are widely known as relatively inexpensive multifaceted catalysts, which are quite efficient in redox reactions and many other applications [26–33]. These materials are typically synthesized by pyrolysis of metal–organic frameworks [22,24,30–32] or using wet impregnation of carbon with complexes of Co with N-heterocycles, followed by pyrolysis [27,33]. In addition, they can be produced by solid-state mixing of Co(II) salts and nitrogen heterocycles with carbon black, followed

by heat treatment. The Co@NC materials thus simply obtained have proven to be effective catalysts in various reactions [34–36], including PDH [25]. Furthermore, according to another example, a hybrid catalyst containing Co-N coordinated compounds supported on oxidized carbon nanotubes (CoN@OCNTs) ensured significant, ~20%, initial conversion of propane and high selectivity to propylene (>95%) at 570 °C [21]. Even higher was the catalytic performance of a more sophisticated CoOx@NC/S-1 composite characterized by spatial isolation of cobalt oxide sites in N-doped carbon, which was prepared by pyrolysis of bimetallic Zn/Co zeolitic imidazole frameworks (ZIFs) loaded on silicalite-1 zeolite [22]. This catalyst provided a propane conversion of 40% and a propylene selectivity of >97% at 600 °C. It is noteworthy that atomically dispersed Co(II)-N_x species [20,21,25], isolated CoO sites [22] or metallic Co nanoparticles [24] have been proposed in each case to be the "real" active sites responsible for the target PDH reaction. It is evident then that the mechanistic aspects of the PDH reaction, catalyzed by Co-N-C materials, are still unclear, though, as in the case of many other catalysts [1–10].

Taking into account the significant general interest in the catalytic behavior of Co-N-C-based materials in a variety of reactions, including the alkane's dehydrogenation, we report here the study on the catalytic activity of Co-N-C/SiO_2 composites toward PDH. Special attention was paid to the definition of the role of the main catalyst components, such as metallic cobalt nanoparticles and subnano-sized cobalt species distributed in mesoporous silica, in the catalytic performance. In contrast to our previous investigation on the activity of Co@NC catalysts in PDH [25], an additional objective of the present work was to examine the possibility of regenerating the spent Co-N-C/SiO_2 catalyst using high-temperature oxidation, which is practically impossible for Co@NC composites in pure form due to their combustibility.

2. Results and Discussion

2.1. Catalysts Characterization

The catalysts denoted as Co-N-C/SiO_2 and Co-N-C/SiO_2-L, differing in the content of Co (9.9 and 0.8%, respectively), were prepared according to the adapted literary procedure [37], by pyrolysis of the silicone gel enriched with Co(II) salt and triethanolamine (see Section 3.2). Figure 1 shows the XRD patterns of the as-synthesized catalysts. Only a single characteristic peak of metallic Co, though comparatively weak and broadened, is present in the XRD pattern of Co-N-C/SiO_2 at around 44.0°, which can be assigned to the (111) plane of Co^0. Such a peak is practically invisible in the case of Co-N-C/SiO_2-L, in accord with the diminished content of Co in this sample. Besides, for both the catalysts a broad diffraction peak is observed at ~23°, which is related to the (111) reflection of the SiO_2.

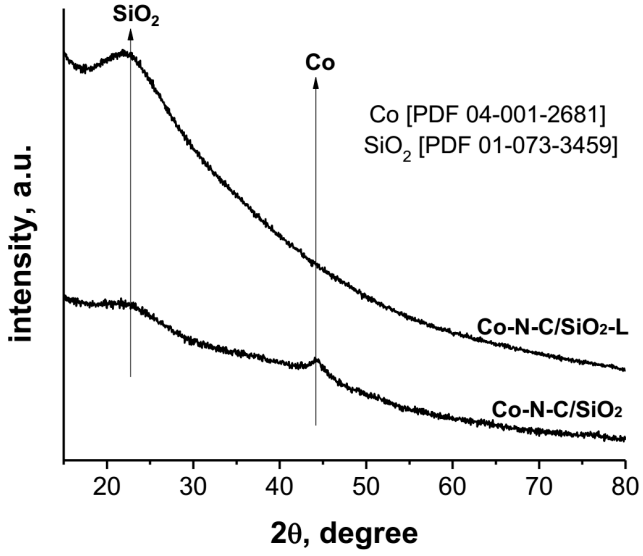

Figure 1. Powder XRD patterns of the prepared catalysts.

Low and higher magnification transmission electron microscopy (TEM) images of Co-N-C/SiO_2 demonstrate the existence of two differing parts of the catalyst (Figure 2a–d). One of which is characterized by significant incorporation of Co^0 particles of about 20 to 40 nm size agglomerated in porous SiO_2 (Figure 2a,b), while the main part of Co-N-C/SiO_2 consists of SiO_2 enriched with Co^0 particles of about 5 to 10 nm size and small particles of CoO_x, which cover metallic cobalt on the catalyst surface or are located separately. In addition, fragments of amorphous and graphitic carbon are also present in the fresh catalyst (Figure 2b–d). No less importantly, according to a high-angle annular dark field scanning transmission electron microscopy (HAADF STEM) and EDX-STEM elemental mapping images, the catalyst contains subnano-sized cobalt species, along with nitrogen and carbon in a well-dispersed state (Figure 3).

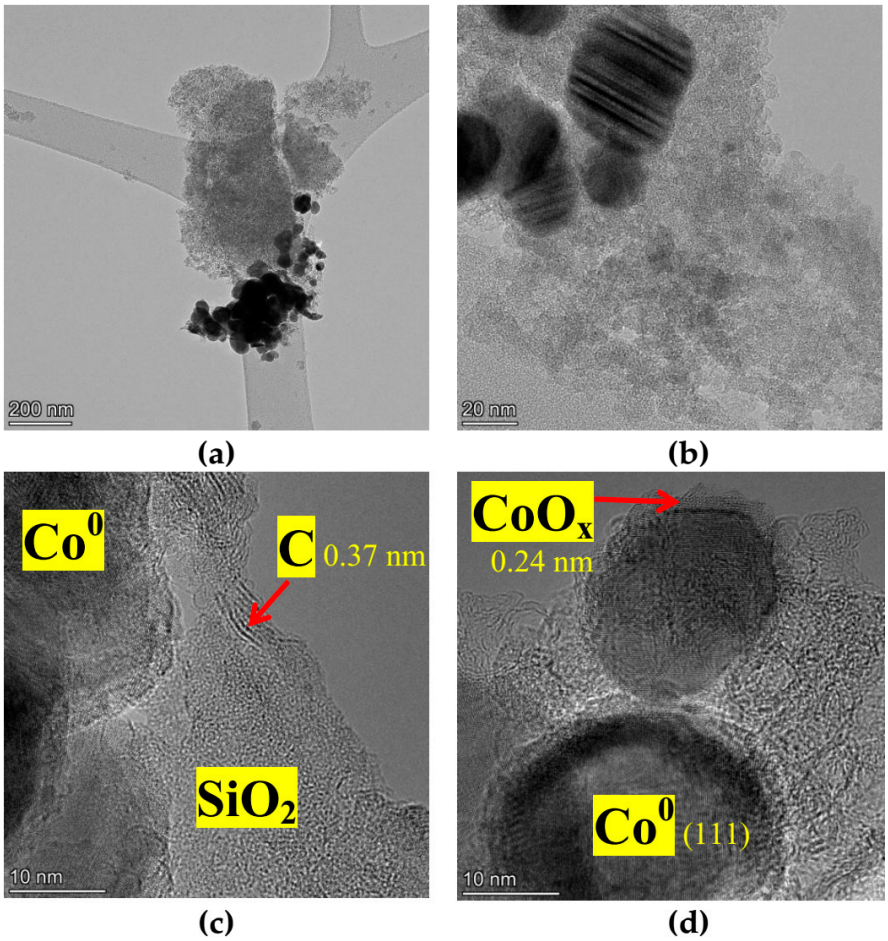

Figure 2. Low (**a**) and higher (**b**–**d**) magnification TEM images of as-synthesized Co-N-C/SiO_2 catalyst, confirming the presence of metallic cobalt particles of different sizes, (**d**) CoO_x on their surface (interlayer spacing of 0.24 nm) and (**c**) fragments of graphitic carbon (interlayer spacing of 0.37 nm).

The wide-range XPS spectra support the presence of Co, C, N, Si and O elements on the surface of Co-N-C/SiO_2 and Co-N-C/SiO_2-L catalysts (Figure S1, Supplementary Materials). The content of these elements and their relative contribution are given in Tables S1 and S2. In the high-resolution Co 2p spectrum, the peaks at 781.7 and ~798 eV are related to Co^{2+}, whereas the peak at 778.2 eV can be assigned to metallic cobalt (Figure 4a). The estimated cobalt content on the surface of Co-N-C/SiO_2 is 2%, which is about 7 times higher than for Co-N-C/SiO_2-L (Table S1). This is in accord with the relative percentage of Co estimated by the X-ray fluorescence (XRF) method (Table 1). However, the surface concentration of other elements in the samples is comparable. The N 1s XPS

spectrum can be deconvoluted into two major peaks corresponding to pyridinic (~398 eV) and pyrrolic/graphitic (~401 eV) functions (Figure 4b). This can be considered essential evidence of the direct connection of nitrogen to carbon.

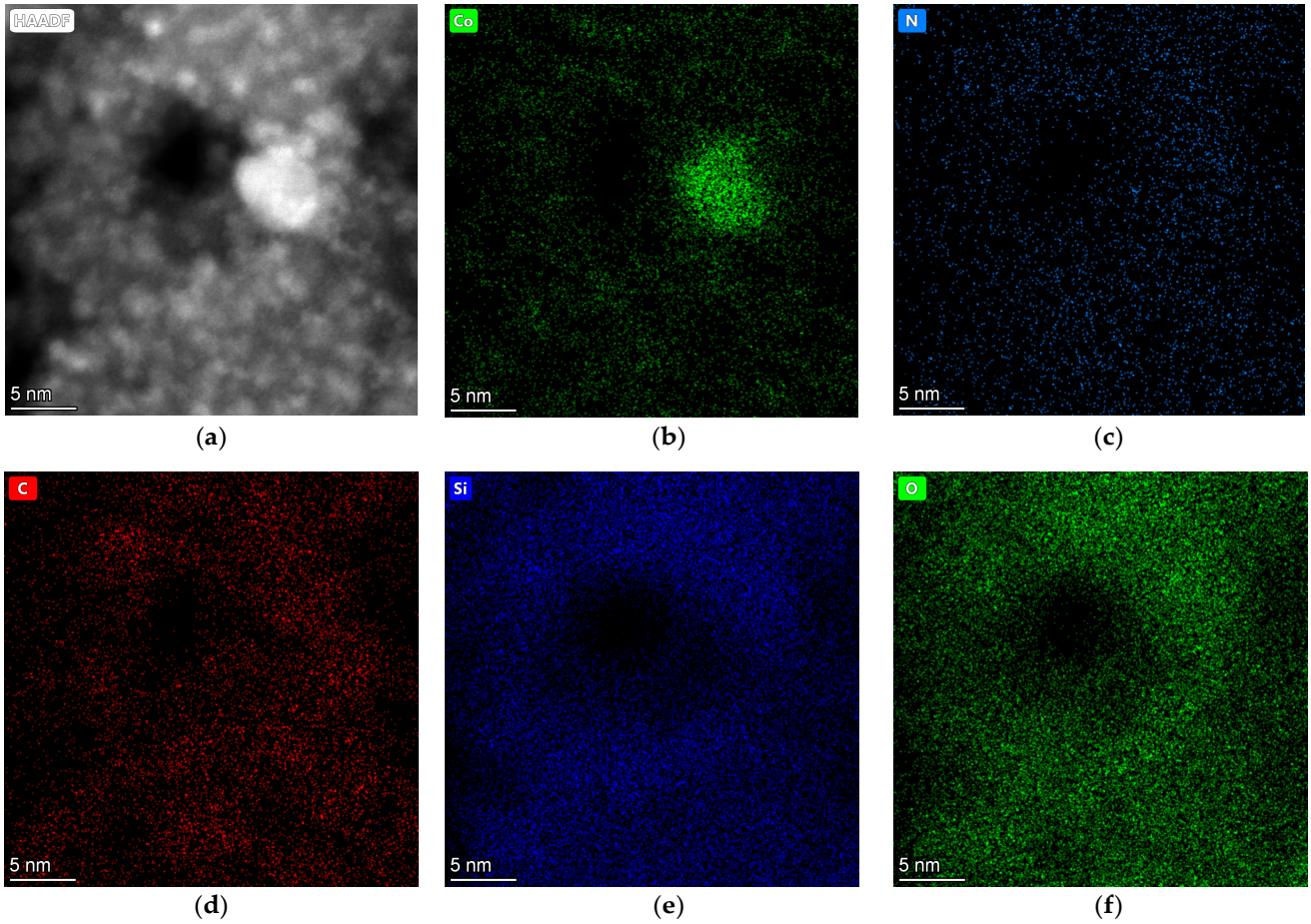

Figure 3. (**a**) HAADF-STEM and related (**b**–**f**) EDX-STEM Co, N, C, Si and O elemental mapping images of typical area of as-synthesized Co-N-C/SiO_2 catalyst.

Table 1. Characterization data for the samples.

Entry	Catalyst	Co (wt%)	S_{BET} (m^2 g^{-1})
1	Co-N-C/SiO_2	9.9	509
2	Co-N-C/SiO_2-L	0.8	424
3	Co/SiO_2	10.9	335
4	N-C/SiO_2	-	412

It should be said also that a peak of Co directly coordinated to nitrogen can be expected on binding energy ~781 eV, while the corresponding peak of N is normally present at 398.8 eV in the Co 2p and N 1s spectra, respectively [24,32]. Obviously, both of these peaks coincide or overlap with close cobalt and nitrogen peaks.

The C 1s region for the catalysts contains the peak at the binding energy of 284.6 eV related to graphitic carbon, though the broad part of this peak between 285 and 288 eV hides the region corresponding to the C–N moiety in N-doped graphite at about 286 eV (Figure 4c). Notably, the carbon content is quite significant, about 20% (Table S1). In general, the XPS characteristics are consistent with the literature [37].

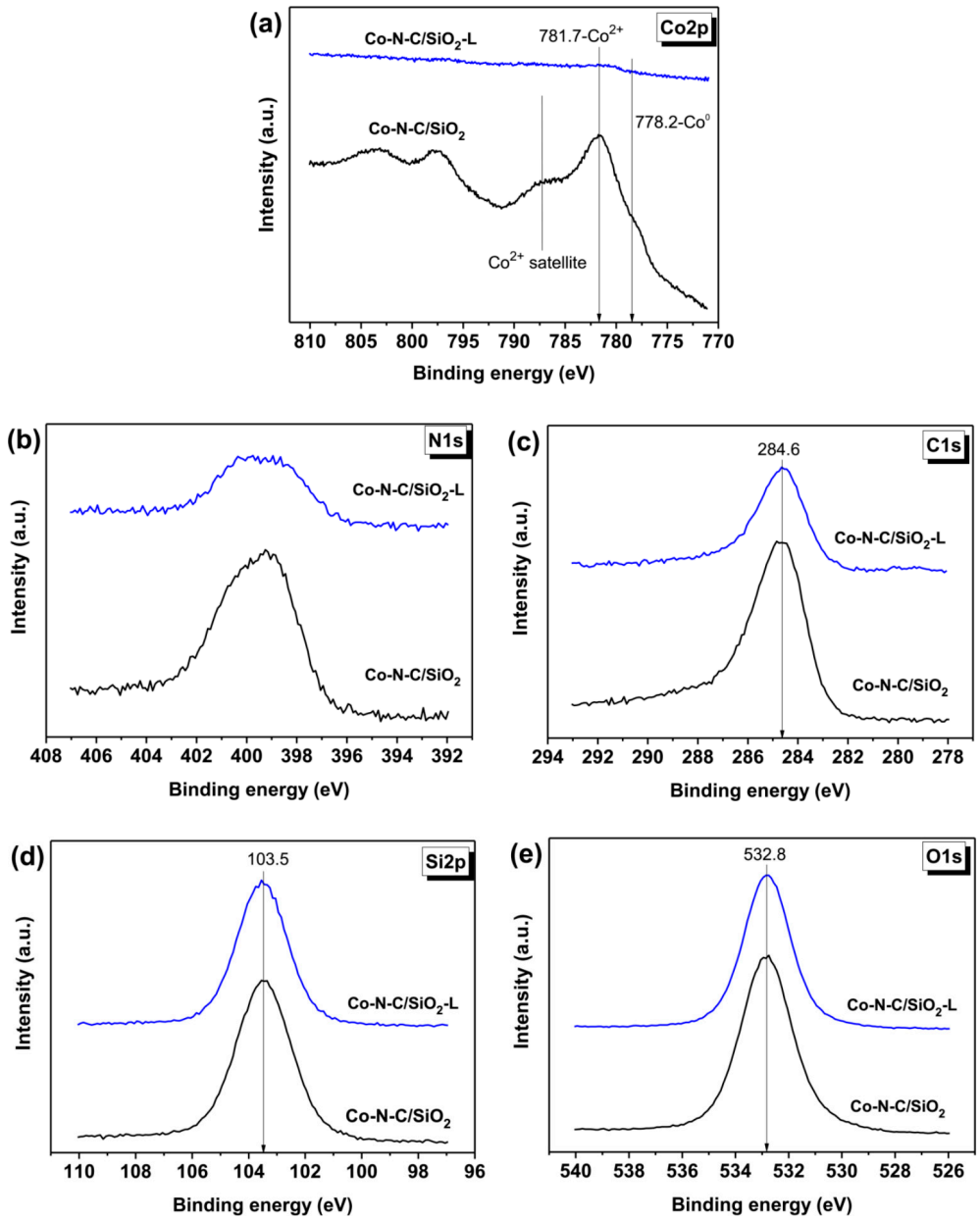

Figure 4. High resolution XPS spectra of (**a**) Co 2p, (**b**) N 1s, (**c**) C 1s, (**d**) Si 2p and (**e**) O 1s of the samples.

The most important conclusion can be drawn from the combined data of XPS, TEM and EDX-STEM, that a significant part of Co is represented by Co^{2+}, which is not subject to reduction to Co^0 under pyrolysis conditions because of coordination with nitrogen, while another part of Co^{2+} remains intact in the form of CoO_x. Nitrogen atoms, in turn, are incorporated into the carbon structure in the pyridinic/pyrrolic form during graphitization, and the latter process is accompanied by deposition on SiO_2.

2.2. Gas-Phase Catalytic Reactions of Propylene in a Flow Reactor

The catalytic performance of the samples was assessed at 600 °C for a 10% propane/N_2 mixture. At the specified reaction conditions, Co-N-C/SiO_2 provides propane conversion of 12 to 16% with selectivity to propylene up to 95% (Figure 5). At that, no significant loss of activity was observed within one hour. As expected, the low-content cobalt catalyst, Co-N-C/SiO_2-L, showed a decrease in the catalytic activity (but not selectivity), affording the propane conversion of 5–7% and selectivity to propylene about 92%. In contrast to the

Co-N-C/SiO_2 and Co-N-C/SiO_2-L catalysts, a cobalt-free sample, N-C/SiO_2, demonstrated notably lower catalytic efficiency, providing propane conversion less than 4% and selectivity to propylene below 80%. It is remarkable that even worse catalytic performance showed cobalt-containing, but a nitrogen-free sample, Co-C/SiO_2, which provoked only cracking reactions and became inactive already in 20 min (Figure S2). These observations clearly indicate the key role of cobalt combined with nitrogen and carbon in the catalytic activity toward PDH reaction.

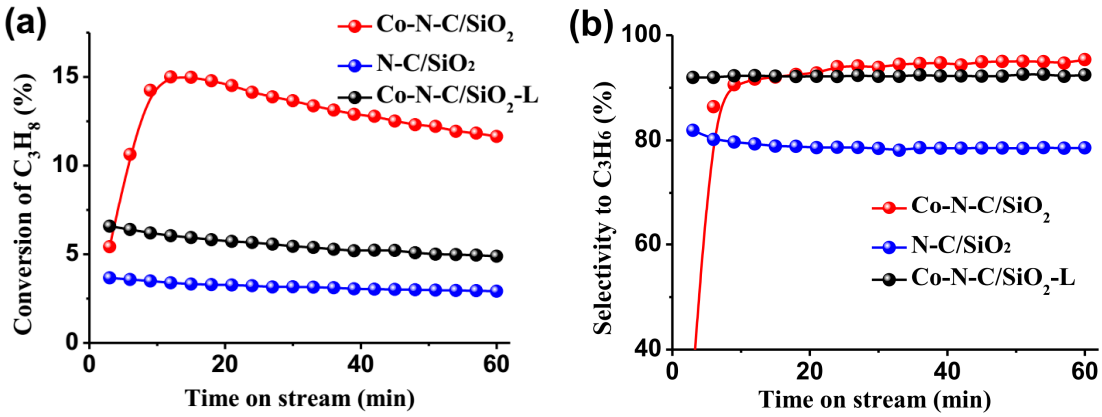

Figure 5. Propane conversion (**a**) and selectivity to propylene (**b**) as functions of time on stream over Co-N-C/SiO_2, Co-N-C/SiO_2-L and N-C/SiO_2 catalysts at T = 600 °C and P = 1 atm. Gas mixture: 10 vol% propane, N_2 balance; GHSV = 7500 mL h^{-1} $g_{cat}{}^{-1}$.

It is found also, that a threefold increase in the loading of Co-N-C/SiO_2 catalyst increases propane conversion twice, up to 30%, which however leads to a diminished (85% to 90%) selectivity to propylene (Figure S3). Nevertheless, this illustrates the principle possibility for further tuning and optimization of the PDH process using Co-N-C/SiO_2 catalysts.

Next, we studied the influence of regeneration on catalytic behavior. Figure 6 shows the difference in activity of the fresh and spent Co-N-C/SiO_2 catalyst, after its regeneration in the N_2/O_2 (60:40 vol.%) flow (6000 mL h^{-1} $g_{cat}{}^{-1}$) at 600 °C during 1 h. The sample thus obtained is designated as Co-N-C/SiO_2-R1. After 3 h of operation in the PDH reaction, this catalyst was regenerated once again, giving a sample designated as Co-N-C/SiO_2-R2. For the purpose of comparison, the regeneration procedure was modified: after the oxidation stage, the catalyst was reduced in the hydrogen flow (6000 mL h^{-1} $g_{cat}{}^{-1}$) at 600 °C for 1 h. It should be noted that both regeneration procedures resulted in significantly higher selectivity to propylene, about 98%. Moreover, despite relatively lower activity during the first hour, these catalysts demonstrated considerably higher long-term stability than the fresh catalyst (Figure 7). In contrast to the parent catalyst, Co-N-C/SiO_2-R1 underwent a quite gradual deactivation process, while Co-N-C/SiO_2-R2 even increased its activity after three hours on stream. It should be mentioned, however, that more or less rapid deactivation of cobalt catalysts is generally typical for the PDH reaction conditions, which resulted from coke deposition and restructure of cobalt species at such a high temperature [24,25,38,39].

Indeed, in accordance with the literature, microscopic images of the spent Co-N-C/SiO_2 catalyst (after 1 h of operation) show significant growth of carbon nanotubes, along with considerable and dense packing carbonization of cobalt nanoparticles (Figure 8). According to STEM-EDX analysis, the content of carbon in various regions of the catalyst notably increased, especially in the areas of agglomerated Co nanoparticles of increased size (cf. Figures S4 and S5). It is also interesting that the grown carbon nanotubes contain a notable amount of cobalt in the form of single atoms and nanoclusters, thus indicating the leaching of Co from the catalyst (Figure S6). This may be an additional mechanism of catalyst deactivation.

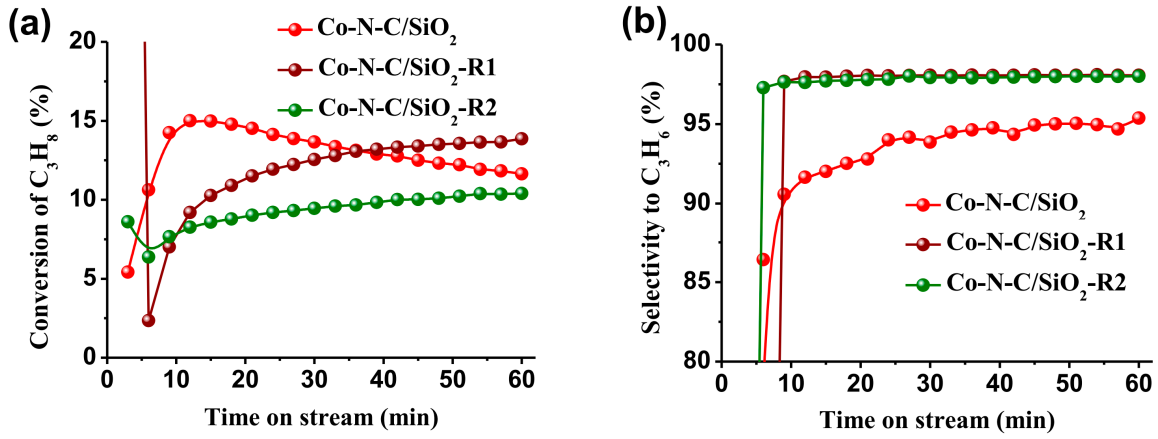

Figure 6. Propane conversion (**a**) and selectivity to propylene (**b**) as functions of time on stream over Co-N-C/SiO_2, Co-N-C/SiO_2-R1 and Co-N-C/SiO_2-R2 catalysts at T = 600 °C and P = 1 atm. Gas mixture: 10 vol% propane, N_2 balance; GHSV = 7500 mL h^{-1} $g_{cat}{}^{-1}$.

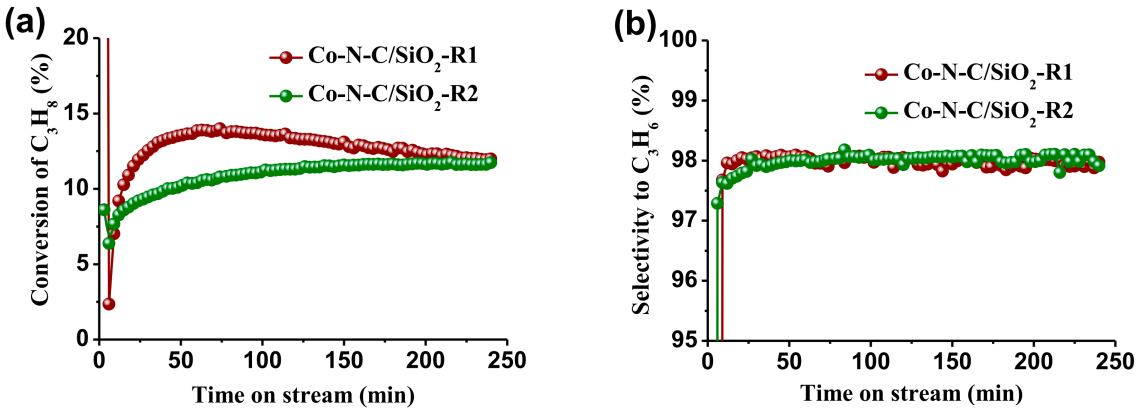

Figure 7. Longer-term conversion of propane (**a**) and selectivity to propylene (**b**) as functions of time on stream over Co-N-C/SiO_2-R1 and Co-N-C/SiO_2-R2 catalysts at T = 600 °C and P = 1 atm. Gas mixture: 10 vol% propane, N_2 balance; GHSV = 7500 mL h^{-1} $g_{cat}{}^{-1}$.

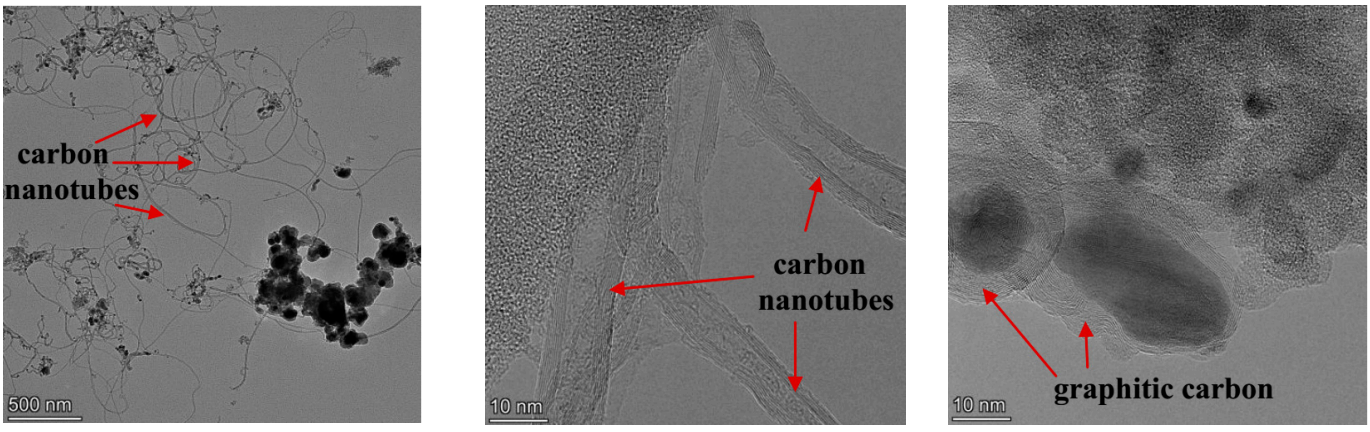

(**a**) (**b**) (**c**)

Figure 8. TEM images of the spent Co-N-C/SiO_2 catalyst (after 1 h of operation at T = 600 °C and P = 1 atm for the gas mixture of 10 vol% propane, N_2 balance, GHSV = 7500 mL h^{-1} $g_{cat}{}^{-1}$) showing (**a**,**b**) the growth of carbon nanotubes; (**c**) significant and dense packing graphitization of cobalt nanoparticles.

The electron microscopic study of the regenerated catalyst Co-N-C/SiO_2-R1 revealed a dramatic difference in its morphology compared with those of the fresh and spent Co-N-C/SiO_2 samples. After the high-temperature oxidation with molecular oxygen, the catalyst became consisted of comparatively small nanoparticles of CoO_x (mainly Co_3O_4) uniformly distributed in porous silica (Figure 9). At that, the silica support retained well-dispersed subnano-sized Co species along with the highly dispersed nitrogen and carbon (Figure 10). According to EDX analysis, the atomic fraction of carbon in the chosen area of the Co-N-C/SiO_2-R1 sample diminished to about 3.5%, which is notably less than in the fresh and especially spent Co-N-C/SiO_2 catalysts (cf. Figures S4 and S5). Obviously, this is caused not only by the burning of carbon in the carbonized areas of the spent catalyst, but also due to the significant, though not exhaustive, oxidation of amorphous and graphite carbon in the original catalyst. In this way, the drastic "regeneration" procedure resulted actually in complete restructure of Co nanoparticles, which underwent redispergation, while the small, subnano-sized Co species coordinated to nitrogen in a carbon frame appeared comparatively resistant.

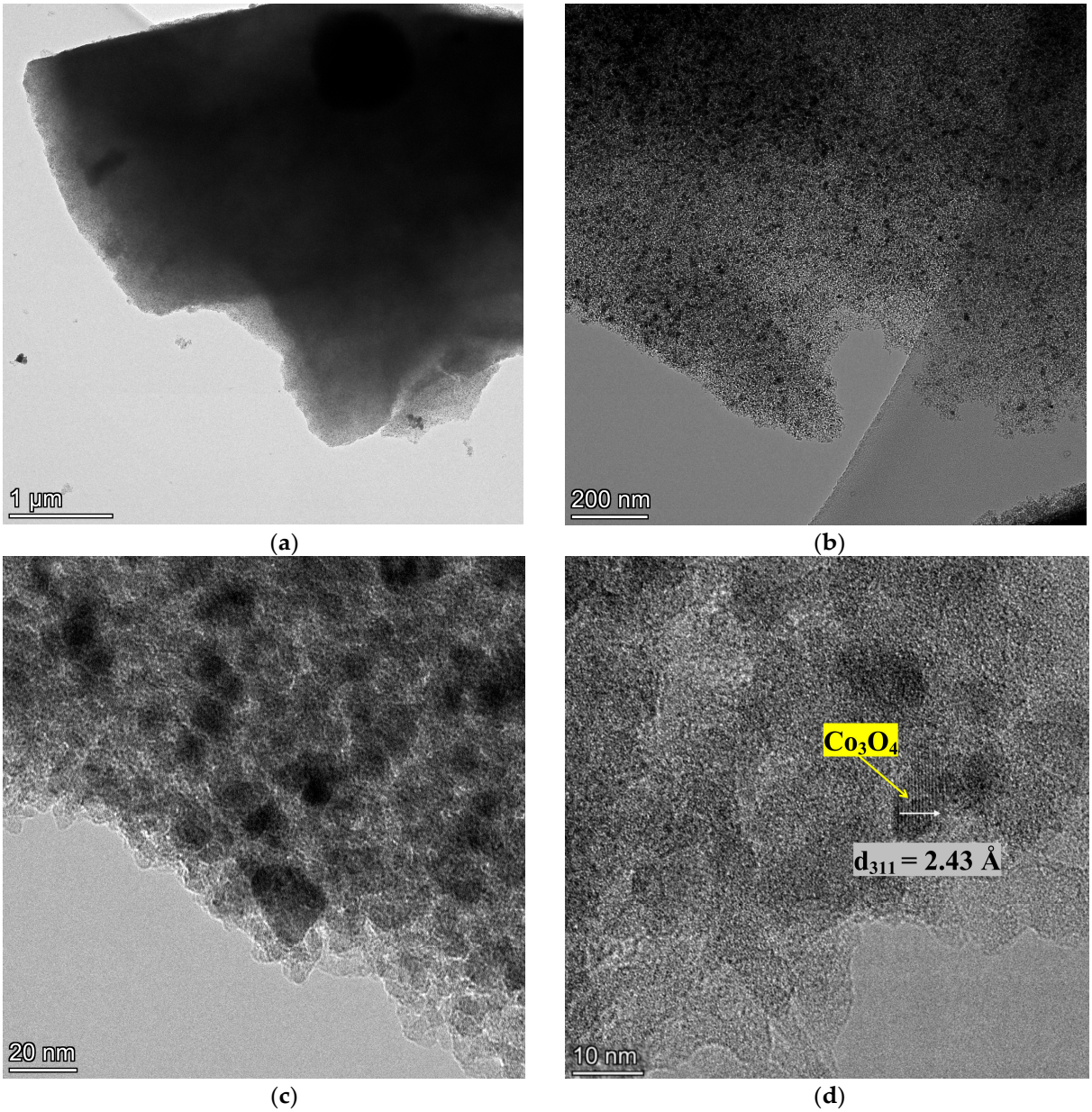

Figure 9. Low (**a**) and higher (**b**–**d**) magnification TEM images of Co-N-C/SiO_2-R1 catalyst.

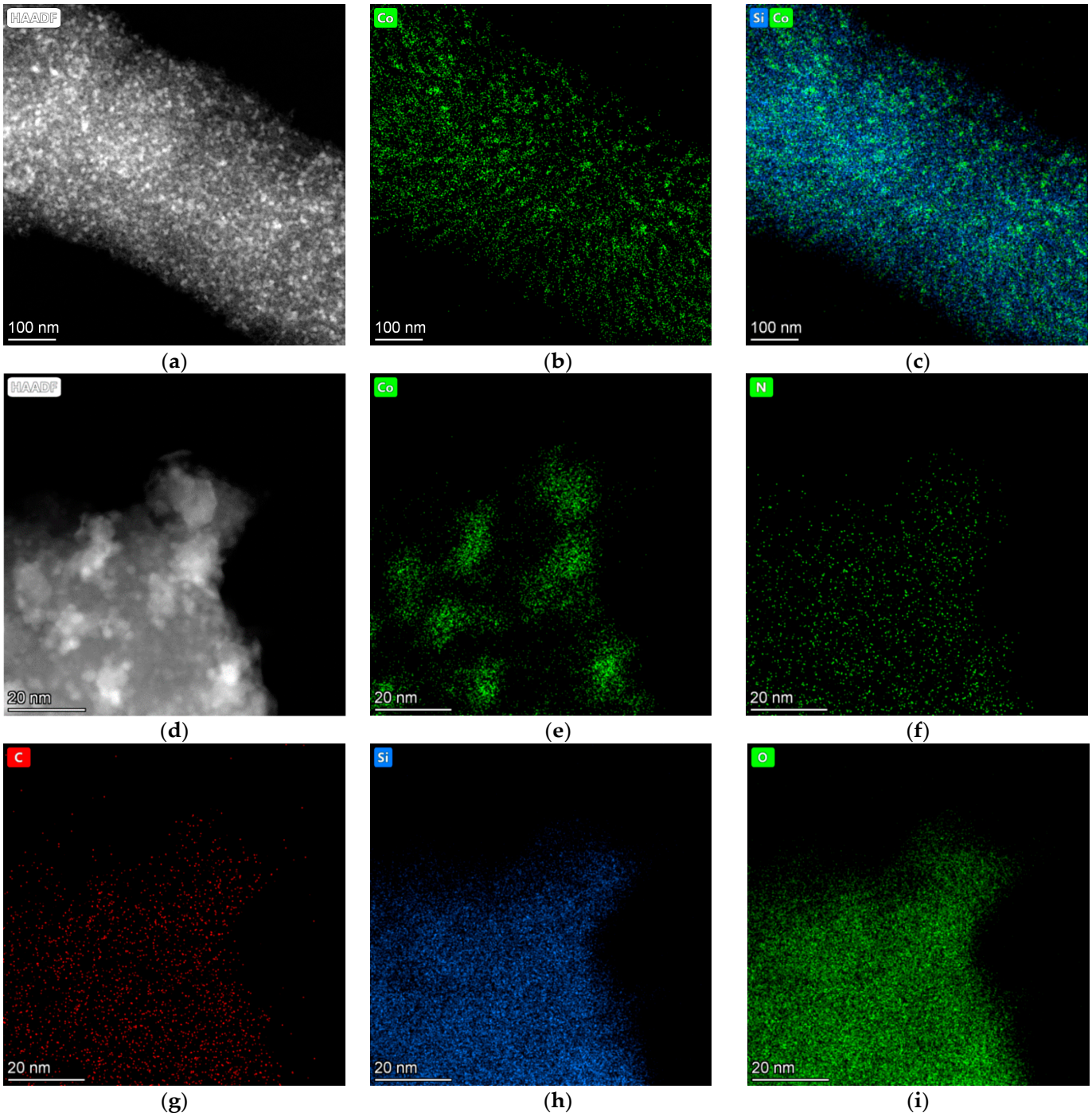

Figure 10. (**a**,**d**) HAADF and related (**b**,**c**,**e**–**i**) EDX-STEM elemental mapping images of Co-N-C/SiO_2-R1.

Considering the peculiarities of the catalytic activity for the Co-N-C/SiO_2, Co-N-C/SiO_2-R1 and Co-N-C/SiO_2-R2 catalysts (Figure 6), one can assume that the comparatively quick deactivation of the fresh sample is related to the significant content of metallic Co^0 nanoparticles, which, as is well known, strongly catalyze the growth of carbon nanotubes and induce their self-carbonization (cf. [25]). Remarkably, these undesirable processes do not proceed this way in the case of "regenerated" catalysts.

It is noteworthy that the relative catalytic activity of Co-N-C/SiO_2 compared with that of the "parent" unsupported Co@NC catalysts reveals some advantage of the latter, which provided propane conversion of 12–23% with selectivity to propylene above 85% upon the same reaction conditions [25]. However, the main drawback of Co@NC catalysts in pure

form is the problem associated with their regeneration, which cannot be solved by either the steam treatment or oxidation to remove selectively the carbon formed during PDH. In contrast, the use of a Co-N-C/SiO_2 composite seems to solve this problem.

As suggested earlier, the active catalytic sites, responsible for the target, PDH reaction, can be the subnano-sized Co species [20–22,25]. Similar species are clearly present in fresh, spent and regenerated Co-N-C/SiO_2 samples. Most probably, they exist in the form of atomically dispersed Co(II)-N_x catalytic sites, as has been shown for a variety of Co@NC materials [20,21,25]. In addition, spatially isolated CoO species in CoOx@NC/S-1 composites could be the active catalytic sites [22]. It is noteworthy that both Co-N-C/SiO_2-R1 and Co-N-C/SiO_2-R2 catalysts required a considerable induction period, about 1 h, to leave on a normal operating mode. This may be explained by the need to reduce, at least partially, nanoparticles of CoO_x present in the regenerated catalysts, which themselves are not considered the actual catalytic sites. We think that their reduction under PDH reaction conditions may lead to an in situ generation of lower oxide forms [40] and ultimately subnano-sized cobalt species, including monoatomic Co^0, which can also catalyze PDH. Otherwise, it will be difficult to explain the gradual increase in propane conversion with high and constant selectivity to propylene. Similarly, the necessity of CoO_x pre-reduction may explain the observed induction period for the Co-N-C/SiO_2 catalyst (Figure 5). In this case, such a period is significantly shorter, about 12 min, due to the much lower CoO_x content in the fresh catalyst.

In this regard, TEM observation of the CoO_x reduction by electron-beam irradiation can be particularly illustrative as the model process for a similar formation of atomic Co on the surface of CoO_x particles upon the PDH reaction conditions (Figure 11). As it can be seen, cobalt atoms are formed on the surface of cobalt oxide.

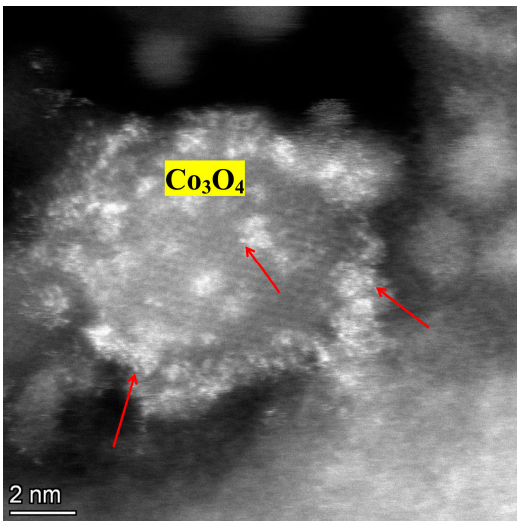

Figure 11. HAADF-STEM image of CoO_x particle on the surface of Co-N-C/SiO_2 subjected to partial reduction with electron-beam irradiation. Red arrows show cobalt atoms formed.

3. Materials and Methods

3.1. Materials

Cobalt(II) nitrate hexahydrate (Fisher Scientific UK, Loughborough, UK), triethanolamine (TEA, 99%, EKOS-1, Moscow, Russia), tetraethyl orthosilicate (TEOS, ≥99%, Sigma-Aldrich, Merck Life Science LLC, Moscow, Russia) and NH_4F (98.5%, Fluorine Salts Chemical Plant LLC, Perm, Russia) were used as received from the chemical suppliers.

3.2. Catalysts Preparation

In a typical procedure, the sample denoted as Co-N-C/SiO_2 was synthesized using an adapted literary approach [37]. To a stirring solution of $Co(NO_3)_2 \cdot 6H_2O$ (1.79 g, 6.15 mmol) in 10 mL of deionized water was added concentrated nitric acid (2 mL). TEA (2.80 g,

18.77 mmol) was added dropwise to the solution, and the mixture was stirred for 10 min, followed by the introduction of TEOS (8 mL) and subsequent stirring for 1 h (until the solution became homogeneous). Then, NH_4F (0.05 g, 1.35 mmol) was introduced and the mixture was stirred until gelation occurred (after 10 to 30 min). The silicone gel obtained was dried under airflow in the hood at room temperature for 48 h. The resultant glass-like solid was milled into grains of about 5 mm in size and dried additionally at 80 °C for 12 h. The dried material was placed in the U-shaped quartz tube and heated at the rate of 3 °C min^{-1} up to 600 °C under Ar flowing at 20 cm^3 min^{-1}. The heat treatment was continued at the reached temperature for 2 h, followed by cooling the sample to room temperature in the argon flow. Finally, the resulting powder material was separated by a magnet to extract the magnetic fraction, representing the catalyst free of very light ash-like components, to provide its easier handling.

For the purpose of comparison, N-C- and Co-free samples and the sample with comparatively low content of Co, denoted as Co-C/SiO_2, N-C/SiO_2 and Co-N-C/SiO_2-L, were also prepared by the same method, but without adding of TEA, $Co(NO_3)_2 \cdot 6H_2O$ and by loading of $Co(NO_3)_2 \cdot 6H_2O$ in the amount of 0.102 g (0.35 mmol), respectively (Table 1).

3.3. Catalysts Characterization Techniques

Powder X-ray diffraction (XRD) patterns of the catalysts were recorded on a Siemens D500 instrument (Siemens, München, Germany) with monochromatized CuKα radiation and θ–2θ focusing geometry. The porous structure parameters were determined from N_2 adsorption isotherms at 77 K on ASAP-2400 (Micromeritics, Norcross, GA, USA) analyzer after degassing the samples at 150 °C to a residual pressure of 30 mTorr (4 Pa). The content of Co element in the samples was measured by X-ray fluorescence using a sequential spectrometer ARL Perform'X with a Rh anode X-ray tube. High-resolution transmission electron microscopy (HRTEM) and scanning transmission electron microscopy (STEM) were obtained with JEM-2010 (JEOL, Tokyo, Japan) and ThemisZ (Thermo Fisher Scientific, Waltham, MA, USA) instruments with accelerating voltage 200 kV and lattice resolutions 0.14 nm and 0.07 nm, respectively. X-ray photoelectron spectra (XPS) were recorded on a SPECS (Berlin, Germany) photoelectron spectrometer using a hemispherical PHOIBOS-150-MCD-9 analyzer (Al K_α radiation, hν = 1486.6 eV, 150 W). The binding energy (BE) scale was pre-calibrated using the positions of the peaks of Au $4f_{7/2}$ (BE = 84.0 eV) and Cu $2p_{3/2}$ (BE = 932.67 eV) core levels. The BE values were corrected by reference to the C 1s internal standard (284.5 eV).

3.4. Catalytic Performance Tests

The PDH reactions were performed in a quartz tube flow reactor with an internal diameter of 7.5 mm. The gas mixture (10 vol% propane balanced with nitrogen) was fed to the reactor at a gas hour space velocity (GHSV) of 7500 mL h^{-1} $g_{cat}{}^{-1}$. Reactions were carried out at atmospheric pressure using a catalyst (0.2 g) mixed with 1 mL of quartz particles (d = 0.45 to 1 mm). The reaction temperature, 600 °C, was controlled inside the reactor with an accuracy of ±0.5 °C. The reaction products were analyzed by an online gas chromatograph (Chromos GC-1000, Chromos Engineering, Dzerzhinsk, Russia) with a flame-ionization detector, using a quartz capillary column of an inner diameter of 0.32 mm and a length of 7 m. The column was prepared by the static high-pressure method, yielding a monolithic layer of porous SiO_2 formed in the process of sol-gel synthesis directly inside the capillary [41]. Prior to the measurements, the catalysts were gradually heated to 600 °C in a flow of N_2 for 1 h. The blank experiments (the quartz particles only) showed propane conversion of ~1.5% and selectivity to propylene of about 57% (Figure S8).

The propane conversion (X) and propylene selectivity (S) were calculated according to the carbon atom balance method:

$$X_{C_3H_8} = \frac{C^0_{C_3H_8} - C_{C_3H_8}}{C^0_{C_3H_8}} \times 100\%;$$

$$S_{C_3H_6} = \frac{C_{C_3H_6}}{C^0_{C_3H_8} - C_{C_3H_8}} \times 100\%;$$

where $C_{C_3H_8}$ and $C_{C_3H_6}$ are the mole flow rates of propane and propylene, respectively. In view of the reaction-induced changes in the gas flow due to the conversion of one molecule of propane into two molecules (propylene and hydrogen) during the reaction, the values of $C_{C_3H_8}$ and $C_{C_3H_6}$ are normalized by carbon balance accordingly.

4. Conclusions

It is shown that a Co-N-C/SiO_2 composite consisting mainly of metallic cobalt nanoparticles and subnano-sized cobalt species uniformly distributed in mesoporous silica can be an effective catalyst in PDH reaction. According to XRD, TEM and XPS characterizations, the Co-N-C/SiO_2 catalyst also contains well-dispersed nitrogen and carbon. The latter structural elements strongly participate in the target PDH reaction. Deactivation of the catalyst proved to be due to its significant carbonization, especially in the areas of increased content of metallic cobalt, catalyzing this process. High-temperature treatment of the catalyst with molecular oxygen effectively removes the accumulated graphitic carbon. Moreover, it results in dramatic changes in the catalyst structure, leading to the formation of cobalt oxide nanoparticles (instead of metallic cobalt), along with their redispersion. The catalyst samples thus developed exhibit more stable catalytic performance, although a longer induction period is required to achieve the usual operating mode. Two kinds of subnano-sized species are suggested as probable catalytic sites. In accordance with the literature, monoatomic Co-N_x/C species are responsible for the target catalytic activity in the case of a fresh Co-N-C/SiO_2 catalyst. The same species, retaining their activity (at least partially), may continue to contribute to the catalysis of PDH after the treatment with oxygen. As an additional catalytic path, participation of atomic Co, generated in situ on the cobalt oxide particles, is also possible.

Supplementary Materials: The following supporting information can be downloaded at: https://www.mdpi.com/article/10.3390/catal12101262/s1, Figure S1: Survey XPS spectra of the samples; Figure S2: Propane conversions and selectivities to propylene over Co-C/SiO_2 as functions of time on stream; Figure S3: Propane conversion and selectivity to propylene over Co-N-C/SiO_2 as functions of time on stream (for the increased catalyst loading); Figure S4: HAADF, EDX-STEM mixed C/Si/Co and separate Co, N, C, Si and O mapping images for a typical area of spent Co-N-C/SiO_2 catalyst; Figure S5: HAADF, EDX-STEM mixed C/Si/Co and separate Co, C, Si and O mapping images for the spent Co-N-C/SiO_2 catalyst for the area of increased content of "oversized" Co nanoparticles; Figure S6: HAADF and EDX-STEM C, Co, Si and O mapping images of a carbon nanotube grown out in the spent Co-N-C/SiO_2 catalyst; Figure S7: HAADF and related EDX-STEM mixed elemental mapping images of Co-N-C/SiO_2-R1, with atomic and mass fraction analysis; Figure S8. Propane conversion and selectivity to propylene over SiO_2 as functions of time on stream (the blank experiment); Table S1: The XPS-derived chemical composition of the samples; Table S2: The XPS-derived atomic fractions of elements in the samples.

Author Contributions: Conceptualization, A.N.C.; investigation, A.N.C. and E.Y.G.; data curation, K.Y.K. and V.I.S.; writing—original draft preparation, K.Y.K.; writing—review and editing, K.Y.K. and V.I.S.; supervision, V.I.S. All authors have read and agreed to the published version of the manuscript.

Funding: This work was supported by the Ministry of Science and Higher Education of the Russian Federation within the governmental order for the Boreskov Institute of Catalysis (project AAAA-A21-121011390008-4).

Data Availability Statement: Not applicable.

Acknowledgments: The studies were carried out using facilities of the shared research center "National center of investigation of catalysts" at Boreskov Institute of Catalysis.

Conflicts of Interest: The authors declare no conflict of interest.

References

1. Zimmermann, H.; Walzl, R. *Ullmann's Encyclopedia of Industrial Chemistry*; Wiley-VCH Verlag GmbH & Co. KGaA: Weinheim, Germany, 2009.
2. Sattler, J.J.H.B.; Ruiz-Martinez, J.; Santillan-Jimenez, E.; Weckhuysen, B.M. Catalytic dehydrogenation of light alkanes on metals and metal oxides. *Chem. Rev.* **2014**, *114*, 10613–10653. [CrossRef] [PubMed]
3. Hu, Z.-P.; Yang, D.; Wang, Z.; Yuan, Z.-Y. State-of-the-art catalysts for direct dehydrogenation of propane to propylene. *Chin. J. Catal.* **2019**, *40*, 1233–1254. [CrossRef]
4. Martino, M.; Meloni, E.; Festa, G.; Palma, V. Propylene Synthesis: Recent Advances in the Use of Pt-Based Catalysts for Propane Dehydrogenation Reaction. *Catalysts* **2021**, *11*, 1070. [CrossRef]
5. Dong, S.; Altvater, N.R.; Mark, L.O.; Hermans, I. Assessment and comparison of ordered & non-ordered supported metal oxide catalysts for upgrading propane to propylene. *Appl. Catal. A-Gen.* **2021**, *617*, 118121. [CrossRef]
6. Chen, S.; Chang, X.; Sun, G.; Zhang, T.; Xu, Y.; Wang, Y.; Pei, C.; Gong, J. Propane dehydrogenation: Catalyst development, new chemistry, and emerging technologies. *Chem. Soc. Rev.* **2021**, *50*, 3315–3354. [CrossRef]
7. Otroshchenko, T.; Jiang, G.; Kondratenko, V.A.; Rodemerck, U.; Kondratenko, E.V. Current status and perspectives in oxidative, non-oxidative and CO_2-mediated dehydrogenation of propane and isobutane over metal oxide catalysts. *Chem. Soc. Rev.* **2021**, *50*, 473–527. [CrossRef]
8. Dai, Y.; Gao, X.; Wang, Q.; Wan, X.; Zhou, C.; Yang, Y. Recent progress in heterogeneous metal and metal oxide catalysts for direct dehydrogenation of ethane and propane. *Chem. Soc. Rev.* **2021**, *50*, 5590–5630. [CrossRef]
9. Wang, Y.; Hu, P.; Yang, J.; Zhu, Y.-A.; Chen, D. C–H bond activation in light alkanes: A theoretical perspective. *Chem. Soc. Rev.* **2021**, *50*, 4299–4358. [CrossRef] [PubMed]
10. Liu, S.; Zhang, B.; Liu, G. Metal-based catalysts for the non-oxidative dehydrogenation of light alkanes to light olefins. *React. Chem. Eng.* **2021**, *6*, 9–26. [CrossRef]
11. Liu, L.; Deng, Q.F.; Agula, B.; Zhao, X.; Ren, T.Z.; Yuan, Z.Y. Ordered mesoporous carbon catalyst for dehydrogenation of propane to propylene. *Chem. Commun.* **2011**, *47*, 8334–8336. [CrossRef] [PubMed]
12. Wang, R.; Sun, X.; Zhang, B.; Sun, X.; Su, D. Hybrid Nanocarbon as a Catalyst for Direct Dehydrogenation of Propane: Formation of an Active and Selective Core–Shell sp^2/sp^3 Nanocomposite Structure. *Chem.-Eur. J.* **2014**, *20*, 6324–6331. [CrossRef] [PubMed]
13. Zhao, Z.; Ge, G.; Li, W.; Guo, X.; Wang, G. Modulating the microstructure and surface chemistry of carbocatalysts for oxidative and direct dehydrogenation: A review. *Chin. J. Catal.* **2016**, *37*, 644–670. [CrossRef]
14. Hu, Z.-P.; Chen, C.; Ren, J.-T.; Yuan, Z.-Y. Direct dehydrogenation of propane to propylene on surface-oxidized multiwall carbon nanotubes. *Appl. Catal. A-Gen.* **2018**, *559*, 85–93. [CrossRef]
15. Hu, Z.P.; Ren, J.T.; Yang, D.; Wang, Z.; Yuan, Z.Y. Mesoporous carbons as metal-free catalysts for propane dehydrogenation: Effect of the pore structure and surface property. *Chin. J. Catal.* **2019**, *40*, 1385–1394. [CrossRef]
16. Zhao, Z.; Dai, Y.; Ge, G.; Wang, G. Explosive Decomposition of a Melamine–Cyanuric Acid Supramolecular Assembly for Fabricating Defect-Rich Nitrogen-Doped Carbon Nanotubes with Significantly Promoted Catalysis. *Chem. Eur. J.* **2015**, *21*, 8004–8009. [CrossRef] [PubMed]
17. Zhao, Z.; Dai, Y.; Ge, G. Nitrogen-doped nanotubes-decorated activated carbon-based hybrid nanoarchitecture as a superior catalyst for direct dehydrogenation. *Catal. Sci. Technol.* **2015**, *5*, 1548–1557. [CrossRef]
18. Song, Y.; Liu, G.; Yuan, Z.Y. N-, P- and B-doped mesoporous carbons for direct dehydrogenation of propane. *RSC Adv.* **2016**, *6*, 94636–94642. [CrossRef]
19. Liu, B.; Zhao, H.; Yang, J.; Zhao, J.; Yan, L.; Song, H.; Chou, L. Fe-containing N-doped porous carbon for isobutane dehydrogenation. *Microp. Mesop. Mater.* **2020**, *293*, 109820. [CrossRef]
20. Xie, J.; Kammert, J.D.; Kaylor, N.; Zheng, J.W.; Choi, E.; Pham, H.N.; Sang, X.; Stavitski, E.; Attenkofer, K.; Unocic, R.R.; et al. Atomically Dispersed Co and Cu on N-Doped Carbon for Reactions Involving C–H Activation. *ACS Catal.* **2018**, *8*, 3875–3884. [CrossRef]
21. Cao, T.; Dai, X.; Li, F.; Liu, W.; Bai, Y.; Fu, Y.; Qi, W. Efficient Non-Precious Metal Catalyst for Propane Dehydrogenation: Atomically Dispersed Cobalt-nitrogen Compounds on Carbon Nanotubes. *ChemCatChem* **2021**, *13*, 3067–3073. [CrossRef]
22. Wang, Y.; Suo, Y.; Ren, J.-T.; Wang, Z.; Yuan, Z.-Y. Spatially isolated cobalt oxide sites derived from MOFs for direct propane dehydrogenation. *J. Colloid Interface Sci.* **2021**, *594*, 113–121. [CrossRef] [PubMed]
23. Wang, Q.; Xu, W.; Ma, Z.; Yu, F.; Chen, Y.; Liao, H.; Wang, X.; Zhou, J. Highly Effective Direct Dehydrogenation of Propane to Propylene by Microwave Catalysis at Low Temperature over Co−Sn/NC Microwave Catalyst. *ChemCatChem* **2021**, *13*, 1009–1022. [CrossRef]
24. Li, Y.-M.; Liu, Z.-Y.; Zhang, Q.-Y.; Wang, Y.-J.; Cui, G.-Q.; Zhao, Z.; Xu, C.-M.; Jiang, G.-Y. Influence of carbonization temperature on cobalt-based nitrogen-doped carbon nanopolyhedra derived from ZIF-67 for nonoxidative propane dehydrogenation. *Pet. Sci.* **2022**. [CrossRef]
25. Chernov, A.N.; Sobolev, V.I.; Koltunov, K.Y. Propane dehydrogenation to propylene over Co@N-doped carbon: Structure-activity-selectivity relationships. *Catal. Commun.* **2022**, *170*, 106495. [CrossRef]
26. Wang, X.; Fu, H.; Li, W.; Zheng, J.; Li, X. Metal (metal = Fe, Co), N codoped nanoporous carbon for efficient electrochemical oxygen reduction. *RSC Adv.* **2014**, *4*, 37779–37785. [CrossRef]

27. Morozan, A.; Goellner, V.; Nedellec, Y.; Hannauer, J.; Jaouen, F. Effect of the Transition Metal on Metal-Nitrogen-Carbon Catalysts for the Hydrogen Evolution Reaction. *J. Electrochem. Soc.* **2015**, *162*, H719–H726. [CrossRef]
28. Liu, W.; Zhang, L.; Yan, W.; Liu, X.; Yang, X.; Miao, S.; Wang, W.; Wang, A.; Zhang, T. Single-atom dispersed Co-N-C catalyst: Structure identification and performance for hydrogenative coupling of nitroarenes. *Chem. Sci.* **2016**, *7*, 5758–5764. [CrossRef]
29. Eisenberg, D.; Slot, T.K.; Rothenberg, G. Understanding oxygen activation on metal- and nitrogen-codoped carbon catalysts. *ACS Catal.* **2018**, *8*, 8618–8629. [CrossRef]
30. Zhang, M.; Zhang, E.; Hu, C.; Zhao, Y.; Zhang, H.; Zhang, Y.; Ji, M.; Yu, J.; Cong, G.; Liu, H.; et al. Controlled Synthesis of Co@N-Doped Carbon by Pyrolysis of ZIF with 2-Aminobenzimidazole Ligand for Enhancing Oxygen Reduction Reaction and the Application in Zn−Air Battery. *ACS Appl. Mater. Interfaces* **2020**, *12*, 11693–11701. [CrossRef] [PubMed]
31. Zhou, Y.-X.; Chen, Y.-Z.; Cao, L.; Lu, J.; Giang, H.-L. Conversion of a metal–organic framework to N-doped porous carbon incorporating Co and CoO nanoparticles: Direct oxidation of alcohols to esters. *Chem. Commun.* **2015**, *51*, 8292–8295. [CrossRef]
32. Gao, Y.; Han, Z.; Hong, S.; Wu, T.; Li, X.; Qiu, J.; Sun, Z. ZIF-67-Derived Cobalt/Nitrogen-Doped Carbon Composites for Efficient Electrocatalytic N_2 Reduction. *ACS Appl. Energy Mater.* **2019**, *2*, 6071–6077. [CrossRef]
33. Li, X.; Surkus, A.-E.; Rabeah, J.; Anwar, M.; Dastigir, S.; Junge, H.; Bruckner, A.; Beller, M. Cobalt Single-Atom Catalysts with High Stability for Selective Dehydrogenation of Formic Acid. *Angew. Chem. Int. Ed.* **2020**, *59*, 15849–15854. [CrossRef] [PubMed]
34. Astrakova, T.V.; Sobolev, V.I.; Koltunov, K.Y. Facile mechanochemical synthesis of Co@NC catalysts for oxidative esterification of benzyl alcohol with methanol. *Catal. Commun.* **2020**, *137*, 105952. [CrossRef]
35. Chernov, A.N.; Astrakova, T.V.; Sobolev, V.I.; Koltunov, K.Y. Liquid versus gas phase dehydrogenation of formic acid over Co@N-doped carbon materials. The role of single atomic sites. *Mol. Catal.* **2021**, *504*, 111457. [CrossRef]
36. Chernov, A.N.; Astrakova, T.V.; Koltunov, K.Y.; Sobolev, V.I. Ethanol dehydrogenation to acetaldehyde over Co@N-doped carbon. *Catalysts* **2021**, *11*, 1411. [CrossRef]
37. Zhang, C.; Zhao, P.; Zhang, Z.; Zhang, J.; Yang, P.; Gao, P.; Gao, J.; Liu, D. Co-N-C supported on SiO_2: A facile, efficient catalyst for aerobic oxidation of amines to imines. *RSC Adv.* **2017**, *7*, 47366–47372. [CrossRef]
38. Dewangan, N.; Ashok, J.; Sethia, M.; Das, S.; Pati, S.; Kus, H.; Kawi, S. Cobalt-Based Catalyst Supported on Different Morphologies of Alumina for Non-oxidative Propane Dehydrogenation: Effect of Metal Support Interaction and Lewis Acidic Sites. *ChemCatChem* **2019**, *11*, 4923–4934. [CrossRef]
39. Dai, Y.; Gu, J.; Tian, S.; Wu, Y.; Chen, J.; Li, F.; Du, Y.; Peng, L.; Ding, W.; Yang, Y. γ-Al_2O_3 sheet-stabilized isolate Co^{2+} for catalytic propane dehydrogenation. *J. Catal.* **2020**, *381*, 482–492. [CrossRef]
40. Kung, H.H. Reduction of oxides. *Stud. Surf. Sci. Catal.* **1989**, *45*, 91–109. [CrossRef]
41. Golovnya, R.V.; Samusenko, A.L.; Mistryukov, E.A. Analysis of polar compounds on PEG-40M/KF glass capillary columns. *J. High Resolut. Chromatogr.* **1979**, *2*, 609–612. [CrossRef]